IAC–20–C1.9.7

Attitude Control Algorithms Aided by Multipoint Statistics and Distributed Measurements Processing in a Swarm of CubeSats

Anton Afanasev
Skolkovo Institute of Science and Technology, Russian Federation, anton.afanasev@skoltech.ru

Anton Ivanov
Skolkovo Institute of Science and Technology, Russian Federation, a.ivanov2@skoltech.ru

Abstract
This study has been conducted as a part of the Skoltech University project to deploy a swarm of 3U CubeSats in LEO. Our previous studies have shown that data exchange in a swarm of satellites may enhance the attitude determination and control system performance in individual satellites by using interpolated distributed measurements of magnetic field in the attitude determination loop. This work takes the concept a step further and investigates a scenario of having within a swarm a subgroup of spacecraft that are equipped with more precise magnetometers than the rest and are employed as a measurement network that serves the precise magnetic field map to the rest of the swarm spacecraft. We consider this servicing network to comprise four spacecraft, whose trajectories ensure the effective spatial configuration for distributed measurements in the region of interest (where the rest of the swarm spacecraft are). Using several interpolation techniques, such as Ordinary and Non-Ordinary Kriging, the servicing satellites provide statistical maps of the surrounding geomagnetic field in the form of semivariograms atlases for each Cartesian coordinate. These maps are then fed to the attitude determination routines of the other swarms satellites and processed by their respective Extended Kalman Filters. Thus, we propose a decentralized communication algorithm between satellites of different groups, based on which every satellite in the swarm improves its ADCS performance. We present our simulation results that show the advantages of the proposed method over the usage of independent controllers in each satellite.
keywords: swarm, CubeSat, Kriging, semivariogram, atlas, magnetic attitude control

1. Introduction

New distributed architectures of space systems provide improved flexibility and adaptability to structural and functional changes [3]. Deployment of the miniature satellites' swarms promises to be fast and inexpensive. These Swarms can comprise simplistic units that detect certain events and exchange signals with each other and even larger more complicated spacecraft that acts as an analysis hub. Swarms or constellations can be employed as distributed artificial intelligence. They can exhibit collective behaviour, such as self-organization, transformability, self-learning and simultaneous sensing over large areas. Farrag [6] for example composed a survey of the technology demonstration in swarm missions. Among those missions we may mention the HERMES (High Energy Rapid Modular Ensemble of Satellites), which is a mission concept, based on a swarm of nanosatellites in low Earth orbit (LEO), hosting simple but fast scintillators to probe the X-ray emission of bright high-energy transients [7]. The swarm mission, our study stems from, is also conceptually a scientific project that is currently under development at Skoltech, aiming to deploy a swarm of four identical 3U CubeSats in a LEO. The CubeSats are to carry gamma-ray sensors, and their collective behavior will be exhibited in detecting gamma-ray bursts and in coordinated attitude control.

We start our study by considering a three-dimensional formation, whose structure is similar to the one proposed in [4], but clusters of closely located satellites are substituted by single points of measurement, thus making the formation a group of four satellites. Two of the satellites are to orbit the Earth in the leader-follower configuration in a near-circular near-polar orbit while the other two must keep the three-dimensional formation nondegenerate.

Having established the orbital motion of the formation spacecraft we proceed implementation of a fully magnetic ADCS and the interpolation of the geomagnetic field distributed measurements in the interior points of the tetrahedron composed of the four satellites. To this end we employ the Kriging interpo-

lation technique [13], which originated in geostatistical analysis, and to the best of our knowledge has not been extensively used in space applications. One of its indisputable advantages over other interpolators is the ability to capture a certain degree of continuity inherent in the spatially distributed properties to be measured.

We build the atlas of the semivariograms, separated into 3 sectors, based on the region of orbit they were constructed upon. Having done that we present simulation results with MSEs of orientation and angular velocity metric, and then compare those results with that of the singleton ADCS, which uses direct measurements of the geomagnetic field. Finally, the conclusion wraps up the paper by discussing the results and prospects of their application.

2. Orbital configuration

The formation of CubeSats in the form of tetrahedron was discussed in our previous work [2]. Here we enumerate main features of the configuration and give quantitative parameters. The formation is deployed at a near polar circular orbit with altitude of 500 km and inclination of 87°. The first satellite is traveling along this orbit, whereas other three satellites occupy relative orbits such that their positions are in the vertices of a non-degenerate tetrahedron.

The motion of closely orbiting satellites in the central gravity field in near circular orbits is described by the Hill-Clohessy-Wiltshire equations [14, 8]. The relative spacecraft dynamics with respect to the orbital reference of the first satellite, which moves along the circular orbit with mean motion ω_0. In this reference frame, z-axis is aligned with the local vertical, y-axis coincides with the normal to the orbital plane, and x-axis (along track) completes the reference frame to the right-handed triad.

The linearized equations describing spacecraft relative motion in near circular orbits are given by

$$\begin{cases} \ddot{x} + 2\omega_0 \dot{z} = u_x, \\ \ddot{y} + \omega_0^2 y = u_y, \\ \ddot{z} - 2\omega_0 \dot{x} - 3\omega_0^2 z = u_z, \end{cases} \tag{1}$$

where $u = \dfrac{\Delta f}{m}$. In the case of free motion, i.e. if $\Delta f = 0$, Eq. (1) admit bounded periodic solutions given by

$$\begin{cases} x(t) = c_1 \cos(\omega_0 t + \alpha_0) + c_3, \\ y(t) = c_2 \sin(\omega_0 t + \beta_0), \\ z(t) = \dfrac{c_1}{2} \sin(\omega_0 t + \alpha_0), \end{cases} \tag{2}$$

where the constants $c_1, c_2, c_3, \alpha_0, \beta_0$ are determined by the initial conditions.

Tetrahedron Formation Initial Conditions					
#	c_1	c_2	c_3	α_0	β_0
1	0	0	0	0	0
2	$\frac{2\rho}{5}$	0	$2\rho\sqrt{\frac{5}{3}}$	0	0
3	2ρ	$\rho\sqrt{5}$	$\rho\sqrt{\frac{5}{3}}$	$-\operatorname{atan}\frac{1}{\sqrt{2}}$	$\operatorname{atan}\sqrt{2} - \pi$
4	2ρ	$\rho\sqrt{5}$	$\rho\sqrt{\frac{5}{3}}$	$\operatorname{atan}\frac{1}{\sqrt{2}}$	$-\operatorname{atan}\sqrt{2}$

Table 1: Initial Conditions for the Tetrahedron Vertices Reference Trajectories

The initial conditions determining the reference trajectories are specified in Table 1. The value of dimensionless parameter ρ, which determines the characteristic distances between the satellites in formation is chosen to be $\rho = 1430$ m for all subsequent simulations. The relative trajectories of the formation are shown in Fig. 1, and the quality change, introduced in (3), is shown in Fig. 2.

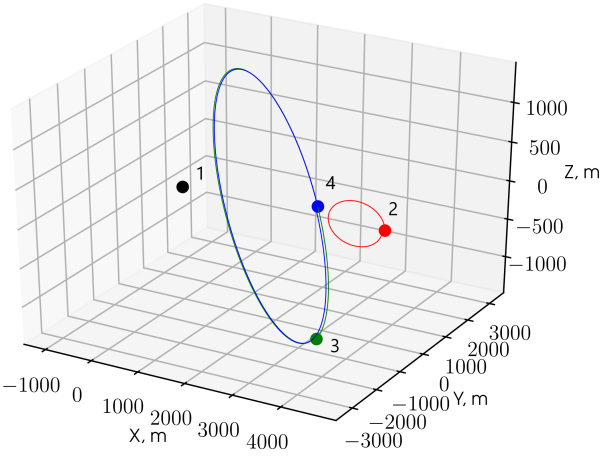

Fig. 1: Relative trajectories of the formation satellites as seen from the orbital frame

The measure of the resulting tetrahedron quality is given as [1, 10]:

$$\mathsf{Q} = 12\frac{(3V)^{2/3}}{L}, \tag{3}$$

where V is the volume of the tetrahedron and L is the sum of squared lengths of all tetrahedron's edges. Q changes between 0 for degenerate configuration and 1 for regular tetrahedrons.

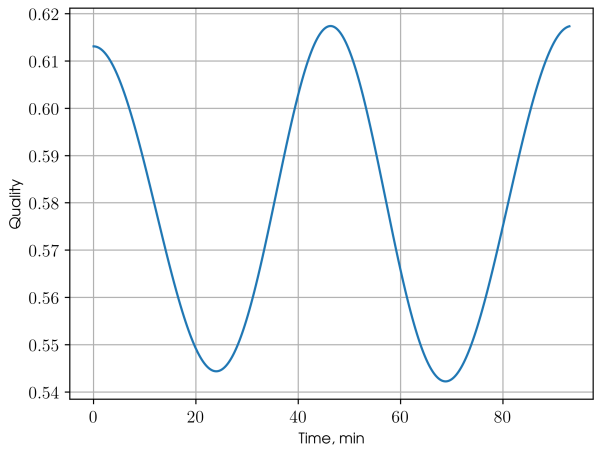

Fig. 2: Formation quality Q

3. Single satellite attitude control

3.1 *Motion and measurements models*

We consider 2 main reference frames: orbital $\mathscr{F}^u \equiv Oxyz$, where z-axis extends through the current position of the satellite, y-axis direction coincides with that of the satellite's center of mass angular momentum and x-axis completes the frame to a right-handed triad; and body-fixed $\mathscr{F}^q \equiv OXYZ$, three axes of which coincide with principle axes of inertia. All vectors represented in those frames are denoted by upper indexes u and q respectively – $\mathbf{r}^u$ and $\mathbf{r}^q$.

The unit quaternion $Q = (q_0, \mathbf{q})$ relates the spacecraft's body-frame $\mathscr{F}^q$ to the orbital frame $\mathscr{F}^u$. Thus representations of any vector $\boldsymbol{r}$ in these two frames $\mathbf{r}^q$ and $\mathbf{r}^u$ are related by

$$\mathbf{r}^u = Q \circ \mathbf{r}^q \circ Q^*,$$

where $Q^* = (q_0, -\mathbf{q})$ is the conjugate of Q.

The satellite is considered to be a rigid body, which complies with the kinematics and dynamics motion equations:

$$\begin{cases} \dot{Q} = \dfrac{1}{2} Q \circ \boldsymbol{\Omega}^q, \\ \mathbf{J}\dot{\boldsymbol{\omega}}^q + \boldsymbol{\omega}^q \times \mathbf{J}\boldsymbol{\omega}^q = \mathbf{T}^q_{\text{ctrl}} + \mathbf{T}^q_{\text{grav}} + \mathbf{T}^q_{\text{dist}} \end{cases} \tag{4}$$

where $\boldsymbol{\omega}^q$ and $\boldsymbol{\Omega}^q$ are absolute and relative angular velocities of the spacecraft, connected via mean-motion ω_0, $\mathbf{J}$ is the diagonalized inertia tensor, $\mathbf{T}^q_{\text{ctrl}}$ is a control torque, $\mathbf{T}^q_{\text{grav}}$ is a gravitational torque and $\mathbf{T}^q_{\text{dist}}$ is a disturbance torque.

The gravity-gradient torque is given by $\mathbf{T}^q_{\text{grav}} = 3\omega_0^2\, \mathbf{e}^q_Z \times \mathbf{J}\mathbf{e}^q_Z$, where $\mathbf{e}^q_Z$ is the ort of Z-axis in $\mathscr{F}^q$. The disturbance torque is modeled as Gaussian noise with zero mean and standard deviation σ_{torque} with corresponding covariance matrix $\boldsymbol{\Sigma}_{\text{torque}} = \sigma^2_{\text{torque}}\mathbf{I}$: $\mathbf{T}^q_{\text{dist}} \sim \mathcal{N}(\mathbf{0}, \boldsymbol{\Sigma}_{\text{torque}})$. And control torque simulates the work of magnetorquer, i.e. equals to vector product of required magnetic moment $\mathbf{m}^q$ and external actual magnetic field $\overline{\mathbf{B}}^q$: $\mathbf{T}^q_{\text{ctrl}} = \mathbf{m}^q \times \overline{\mathbf{B}}^q$.

The magnetic moment is computed with the aid of the well-known Lyapunov-based algorithm [9]

$$\mathbf{m}^q = k_\omega \Delta\boldsymbol{\Omega}^q \times \mathbf{B}^q + k_s \mathbf{S}^q \times \mathbf{B}^q, \tag{5}$$

where $\Delta\boldsymbol{\Omega}^q = \boldsymbol{\Omega}^q - \boldsymbol{\Omega}^q_{\text{req}}$ is the angular velocity error, $\mathbf{S}^q = 4q_0\mathbf{q}$ is the attitude error corresponding to the error quaternion Q, $\mathbf{B}^q$ is the on-board estimate of the external geomagnetic field, k_ω and k_s are the control gains.

The difference between the on-board estimate of the external geomagnetic field $\mathbf{B}^q$ and the actual current field $\overline{\mathbf{B}}^q$ can reach values of $\sigma_{\text{env}} = 300$ nT, if, as in this research, the IGRF-13 model of the magnetic field [5] is used, since the OBC model is usually reduced. That's why we model the difference between 2 field vectors as the Gaussian noise with 0 mean and and covariance matrix $\boldsymbol{\Sigma}_{\text{env}} = \sigma^2_{\text{env}}\mathbf{I}$: $\overline{\mathbf{B}}^q - \mathbf{B}^q \sim \mathcal{N}(\mathbf{0}, \boldsymbol{\Sigma}_{\text{env}})$.

The measurement of the geomagnetic field is occured via magnetometers, which have bias $\mathbf{B}^q_{\text{bias}}$ and standard deviation σ_{meas} with corresponding covariance matrix $\boldsymbol{\Sigma}_{\text{meas}} = \sigma^2_{\text{meas}}\mathbf{I}$. So, measurements $\widetilde{\mathbf{B}}^q$ also modeled as Gaussian noise: $\widetilde{\mathbf{B}}^q - \overline{\mathbf{B}}^q \sim \mathcal{N}(\mathbf{B}^q_{\text{bias}}, \boldsymbol{\Sigma}_{\text{meas}})$. In current research the bias is considered to be zero.

3.2 *Extended Kalman Filter*

The Kalman filter represents recursive estimation of the state vector $\mathbf{X}(t)$ of an a dynamical system [11]. To calculate the current i^{th} state of the system $\mathbf{X}_i = \mathbf{X}(t_i)$ it is necessary to obtain the current measurement $\mathbf{z}_i = \mathbf{z}(t_i)$ and know the previous state $\mathbf{X}_{i-1} = \mathbf{X}(t_{i-1})$. Kalman filter also operates with estimates of the uncertainty of the state vector in the form of covariance matrix $\mathbf{P}_i = \mathbf{P}(t_i)$.

Since our system (4) is nonlinear, the Extended Kalman Filter (EKF) should be used. The general form of a nonlinear continuous system with discrete measurements for EKF is written as follows:

$$\begin{aligned} \dot{\mathbf{X}}(t) &= f(\mathbf{X}(t)) + \mathbf{G}\mathbf{w}(t) \\ \mathbf{z}_i &= h(\mathbf{X}_i) + \mathbf{v}_i \end{aligned} \tag{6}$$

where function f is the evolution of vector $\mathbf{X}$, function h is the measurement model of vector $\mathbf{X}$, $\mathbf{w}$ and $\mathbf{v}$ are process and observation noises, respectively, with

normal distribution and covariance matrices $\mathbf{\Sigma_w}$ and $\mathbf{\Sigma_v}$, and $\mathbf{G}$ is the matrix of the process noise $\mathbf{w}$ influence on the state-space vector $\mathbf{X}$.

Let $\widetilde{\mathbf{X}}$ and $\widehat{\mathbf{X}}$ denote the predicted (or extrapolated) and corrected (or filtered) estimates of the state-space vector, respectively, and let $\widetilde{\mathbf{P}}$ and $\widehat{\mathbf{P}}$ be the corresponding covariance matrices. The predicted value of the vector is obtained out of the corrected one in the previous time step via the evolution function f from (6):

$$\begin{aligned} &\dot{\mathbf{X}}(t) = f\left(\mathbf{X}(t)\right) \\ &\text{w.r.t. } \mathbf{X}(t_{i-1}) = \widehat{\mathbf{X}}_{i-1} \end{aligned} \quad \Longrightarrow \quad \mathbf{X}(t_i) = \widetilde{\mathbf{X}}_i \tag{7}$$

Let $\mathbf{F}_i$ and $\mathbf{H}_i$ be evolution and observation matrices, respectively:

$$\mathbf{F}_i = \left.\frac{\partial f}{\partial \mathbf{X}}\right|_{\mathbf{X}=\widehat{\mathbf{X}}_{i-1}} \qquad \mathbf{H}_i = \left.\frac{\partial h}{\partial \mathbf{X}}\right|_{\mathbf{X}=\widetilde{\mathbf{X}}_i} \tag{8}$$

The covariance matrix of the discrete-time process noise with respect to state-space vector is given by

$$\mathbf{\Sigma_{Gw}} = \int_{t_{i-1}}^{t_i} \mathbf{\Phi}_i \mathbf{G} \mathbf{\Sigma_w} \mathbf{G}^\top \mathbf{\Phi}_i^\top dt, \tag{9}$$

where $\mathbf{\Phi}_i$ is the transition matrix between steps $i-1$ and i:

$$\mathbf{\Phi}_i = \exp\left[\mathbf{F_i}\left(t_i - t_{i-1}\right)\right] \tag{10}$$

Covariance matrix prediction $\widetilde{\mathbf{P}}_i$ on the basis of Eqs. (10) and (9) becomes as follows:

$$\widetilde{\mathbf{P}}_i = \mathbf{\Phi}_i \widehat{\mathbf{P}}_{i-1} \mathbf{\Phi}_i^\top + \mathbf{\Sigma_{Gw}} \tag{11}$$

Having completed the prediction step with Equations (7) and (11) we proceed to the correction step, which is given by:

$$\begin{aligned} \mathbf{K}_i &= \widetilde{\mathbf{P}}_i \mathbf{H}_i^\top \left(\mathbf{H}_i \widetilde{\mathbf{P}}_i \mathbf{H}_i^\top + \mathbf{\Sigma_v}_i\right) \\ \widehat{\mathbf{X}}_i &= \widetilde{\mathbf{X}}_i + \mathbf{K}_i \left(\mathbf{z}_i - h\left(\widetilde{\mathbf{X}}_i\right)\right) \\ \widehat{\mathbf{P}}_i &= \left(\mathbf{I} - \mathbf{K}_i \mathbf{H}_i\right) \widetilde{\mathbf{P}}_i \end{aligned} \tag{12}$$

where $\mathbf{K}$ is Kalman gain matrix.

The state-space vector in our case is concatenation of quaternion and angular velocity: $\mathbf{X} = \begin{pmatrix}\mathbf{q} & \boldsymbol{\omega}^q\end{pmatrix}^\top$. After the linearization of dynamics and measurement models we get matrices:

$$\mathbf{F} = \begin{pmatrix} \mathbf{0}_{3\times3} & \frac{1}{2}\mathbf{I}_{3\times3} \\ \mathbf{0}_{3\times3} & \mathbf{0}_{3\times3} \end{pmatrix} \qquad \mathbf{H}_i = \begin{pmatrix} 2\mathbf{W}_{h(\widetilde{\mathbf{x}}_i)} & \mathbf{0}_{3\times3} \end{pmatrix}$$

where $\mathbf{W_s}$ is a skew-symmetric matrix for vector $\mathbf{s}$ and $h(\mathbf{X})$ is conversion of orbital magnetic field value into the body-fixed frame: $Q^* \circ \mathbf{B}^u \circ Q$.

The process noise $\mathbf{w}$ is clearly $\mathbf{T}^q_{\text{dist}}$ with matrix $\mathbf{G}$ equal $\begin{pmatrix}\mathbf{0}_{3\times3} & \mathbf{J}^{-1}\end{pmatrix}^\top$. The observation noise $\mathbf{v}$ is represented by measurements $\mathcal{N}\left(\mathbf{B}^q_{\text{bias}}, \mathbf{\Sigma}_{\text{meas}}\right)$.

The CubeSat's tensor of inertia is $\mathbf{J} = \operatorname{diag}\left(0.011, 0.014, 0.009\right) \text{kg} \cdot \text{m}^2$. The output of the magnetorquers is limited by $|\mathbf{m}_{\max}| = 0.1 \text{ A} \cdot \text{m}^2$. The control loop time settings are $t_{\text{ctrl}} = 5$ s and $t_{\text{meas}} = 1$ s. The controller gains are tuned to $(k'_\omega, k_s) = (45, 10)\ \frac{\text{N} \cdot \text{m}}{\text{T}^2}$.

Initial state-space vector: $\mathbf{X}_0 = \mathbf{0}_{6\times1}$. These values are used to initialize both the dynamical model and the Kalman filter. Initial covariance matrix: $\mathbf{P}_0 = \operatorname{diag}\left(\sigma^2_{q_0}, \sigma^2_{q_0}, \sigma^2_{q_0}, \sigma^2_{\omega_0}, \sigma^2_{\omega_0}, \sigma^2_{\omega_0}\right)$, where σ_{q_0} and σ_{ω_0} are assumptions of the maximum (or big enough) errors of quaternions and angular velocities respectively. In this study $\sigma_{q_0} = 1$ and $\sigma_{\omega_0} = \frac{\pi}{18}\left[\frac{\text{rad}}{\text{s}}\right]$.

Noise parameters: standard deviation of torque noise $\sigma_{\text{torque}} = 5 \text{ nN} \cdot \text{m}$; magnetometer bias $\mathbf{B}_{\text{bias}} = 0$; standard deviation of measurement noise $\sigma_{\text{meas}} = 100$ nT; standard deviation of environmental noise $\sigma_{\text{env}} = 300$ nT.

The result of the simulation for a single satellite is shown in the figure 3.

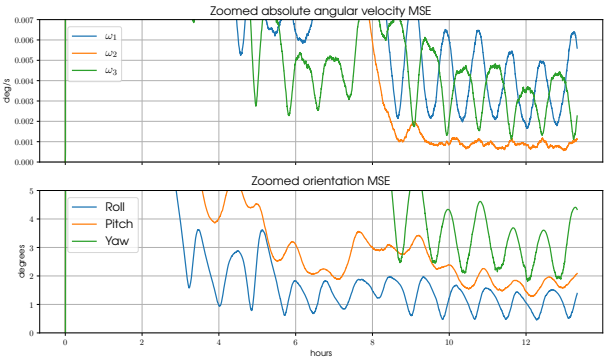

Fig. 3: Orientation MSEs for a single satellite ADCS with EKF

4. Attitude control in a swarm

4.1 *Data exchange and interpolation*

For the swarm scenario there are multiple of orbital and body-fixed frames – $\mathscr{F}^u$ and $\mathscr{F}^q$. In that case we shall enumerate them according to the number of satellites in the swarm: $\mathscr{F}^u_j$, $\mathscr{F}^q_j$ – orbital and

body-fixed reference frames of the j^{th} satellite in the swarm. Respective vectors in those frames have the following view: $\mathbf{r}^{u_j}$, $\mathbf{r}^{q_j}$.

The magnetic field is measured by the magnetometers of each satellite in the swarm. Those measurements $\widetilde{\mathbf{B}}_j^{q_j}$ are in body frame $\mathscr{F}_j^q$.

The obtained values are then converted to the respective orbital reference frame of the j^{th} satellite $\mathscr{F}_j^u$ with the current quaternion Q_j:

$$\widetilde{\mathbf{B}}_j^{u_j} = Q_j \circ \widetilde{\mathbf{B}}_j^{q_j} \circ Q_j^* \tag{13}$$

To interpolate given values all vectors should be converted to the single reference frame, which is orbital reference frame of the first satellite $\mathscr{F}_1^u$, stationary in the relative motion of the whole formation.

The conversion between $\mathscr{F}_j^u$ and $\mathscr{F}_1^u$ is carried out via DCM, which requires the position of the j^{th} satellite in $\mathscr{F}_1^u$. To fulfill this condition, each satellite, in addition, sends to chosen CubeSat its position $\mathbf{R}_j^{u_1}$ to form the DCM $\mathbf{A}_{j\to 1}^u$. So, the measurements are converted:

$$\widetilde{\mathbf{B}}_j^{u_1} = \mathbf{A}_{j\to 1}^u \widetilde{\mathbf{B}}_j^{u_j} \tag{14}$$

Finally, the chosen CubeSat estimates the value of the magnetic field in its own location $\widehat{\mathbf{B}}_j^{u_1}$, using the Kriging algorithm with known tuples of (location, parameter) of all other satellites in the form $\left(\mathbf{R}_j^{u_1}, \widetilde{\mathbf{B}}_j^{u_1}\right)$. The procedure repeats for all satellites until we get all 4 estimates for each one: $\widehat{\mathbf{B}}_1^{u_1}, \widehat{\mathbf{B}}_2^{u_1}, \widehat{\mathbf{B}}_3^{u_1}, \widehat{\mathbf{B}}_4^{u_1}$. Those estimates are all in the orbital frame of the first CubeSat $\mathscr{F}_1^u$. Estimates after converted back to the body-fixed frame of their own satellites via known DCMs and quaternions:

$$\begin{aligned} \widehat{\mathbf{B}}_j^{u_j} &= \left(\mathbf{A}_{j\to 1}^u\right)^\top \widehat{\mathbf{B}}_j^{u_1} \\ \widehat{\mathbf{B}}_j^{q_j} &= Q_j^* \circ \widehat{\mathbf{B}}_j^{u_j} \circ Q_j \end{aligned} \tag{15}$$

Acquired estimates $\widehat{\mathbf{B}}_j^{q_j}$ are used as measurements $\mathbf{z}$ in EKF.

4.2 *Kriging*

Kriging algorithms are a family of linear regression methods to estimate point values at any location within a given region [12], which not only constructs predicted values surface, but also provides representation of the reliability of such values.

The estimator in Kriging is weighted sum of measurements in the vicinity of the interpolated point:

$$\widehat{\mathbf{B}}(\mathbf{R}_0) = \sum_{j=1}^{n} \kappa_j \widetilde{\mathbf{B}}(\mathbf{R}_j) \tag{16}$$

where $\mathbf{R}_0$ is the interpolated point, $\widehat{\mathbf{B}}$ is the predicted value of the measured parameter, $\mathbf{R}_j$ are the points available in the vicinity of interpolated one, $\widetilde{\mathbf{B}}$ is the measurement of geomagnetic field, κ_j are the weights, reflecting the spatial correlation between $\mathbf{R}_j$ and $\mathbf{R}_0$, n is the number of available points.

Assuming unbiasedness of the estimator $\left(\mathsf{E}\left[\widehat{\mathbf{B}}(\mathbf{R}_0)\right] = \mathsf{E}\left[\widetilde{\mathbf{B}}(\mathbf{R}_0)\right]\right)$, and minimizing the variance of the estimator prediction $\left(\min \mathsf{D}\left[\widehat{\mathbf{B}}(\mathbf{R}_0) - \widetilde{\mathbf{B}}(\mathbf{R}_0)\right]\right)$, we acquire the system of equations on weights κ_j and Lagrange multiplier $\varkappa$ (E is expected value and D is variance):

$$\begin{cases} \sum\limits_{j=1}^{n} \kappa_j \gamma(\mathbf{R}_i - \mathbf{R}_j) + \varkappa = \gamma(\mathbf{R}_i - \mathbf{R}_0), \\ \sum\limits_{j=1}^{n} \kappa_j = 1. \end{cases} \tag{17}$$

where $\gamma(h)$ is the semivariance, which by definition is $\gamma(\mathbf{R}_i - \mathbf{R}_j) = \frac{1}{2}\mathsf{D}\left[\widetilde{\mathbf{B}}(\mathbf{R}_i) - \widetilde{\mathbf{B}}(\mathbf{R}_j)\right]$.

So, to calculate weights κ_j we should know values of the semivariance between measurement points. Those values are acquired via semivariograms.

4.3 *Atlas of semivariograms*

To collect the information about the semivariance of the measured parameter in the region, the empirical semivariogram is built. Empirical semivariogram accepts the distance between measured points h as an argument and returns the approximate semivariance for points located at a distance h from each other:

$$\begin{aligned} &\forall \mathbf{R}_i, \mathbf{R}_j : \quad |\mathbf{R}_i - \mathbf{R}_j| = h \\ &\gamma(h) = \frac{1}{2n_h} \sum_{(i,j)=1}^{n_h} \left(\widetilde{\mathbf{B}}(\mathbf{R}_i) - \widetilde{\mathbf{B}}(\mathbf{R}_j)\right)^2, \end{aligned} \tag{18}$$

where n_h is the total number of sampled points pairs.

Then empirical semivariogram can be approximated with some model function. This is necessary, due to discontinuity of $\gamma(h)$ in Eq. (18).

In this research we also introduce the separation of the orbit on 3 sectors with respective semivariograms. In comparison with previous study [2], where we used only one semivariogram for the whole orbit, there are 3 sources of measurement points, which is more favorable in the context of heterogeneity of the geomagnetic field. The separation is shown in he figure 4.

Collecting measurement data from cubes with size 50 km and centers in the points of orbit with argu-

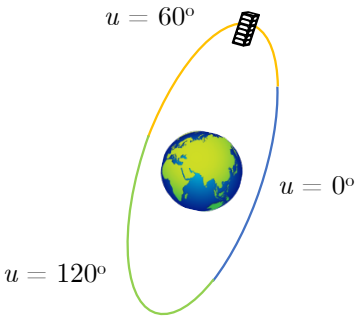

Fig. 4: The separation of the orbit on sectors with different semivariograms

ments of latitude 0°, 60° and 120°, we acquire empirical semivariograms, shown in the figure 5.

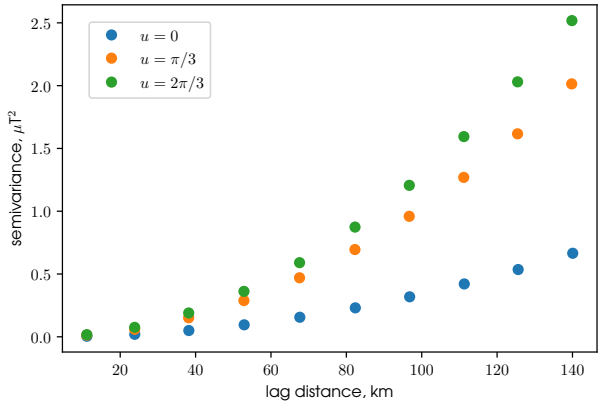

Fig. 5: Atlas of semivariograms for 3 sectors

There are a lot of model functions, but the best one in terms of fitting accuracy is powered exponential one with following view:

$$\gamma(h) = \begin{cases} c_0 + c\left(1 - \exp\left[-\left(\frac{h}{a}\right)^{\nu}\right]\right), & h > 0 \\ 0, & h = 0 \end{cases} \tag{19}$$

where c_0, c, a and ν are parameters of the model.

Fitting the model from Eq. (19) into the empirical semivariograms from figure 5 gives parameters distribution, listed in the table 2.

The comparison of the MSEs of the measurements $\widetilde{\mathbf{B}}$ and interpolated estimates $\widehat{\mathbf{B}}$ in relation to the actual value of the magnetic field $\overline{\mathbf{B}}$ for one satellite from swarm is drawn in the figure 6.

It's clear from the figure that the interpolation gives considerable decrease to the observation noise. The enhancement is best seen in the case of magnetic

u, deg	c_0, μT^2	c, μT^2	a, km	ν
0	0.01	1.15	441	2.54
60	0.04	2.48	364	2.77
120	0.08	4.15	380	2.76

Table 2: Parameters of the powered exponential semivariogram model for 3 sectors of orbit

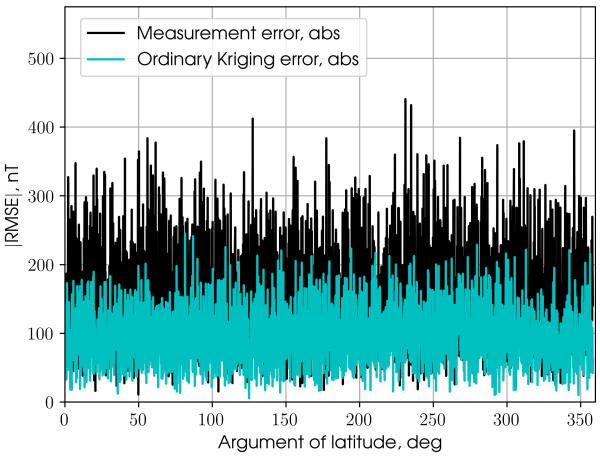

Fig. 6: Measurements vs Interpolated estimates MSEs in absolute value

storms, when the interpolation with different sources eliminates big bias of the storm.

Using same parameters as in the Section 3, but replacing measurements $\widetilde{\mathbf{B}}$ with interpolated estimates $\widehat{\mathbf{B}}$ in the ADCS of a satellite, we computed the MSEs for swarm scenario, results of which are in the figure 7.

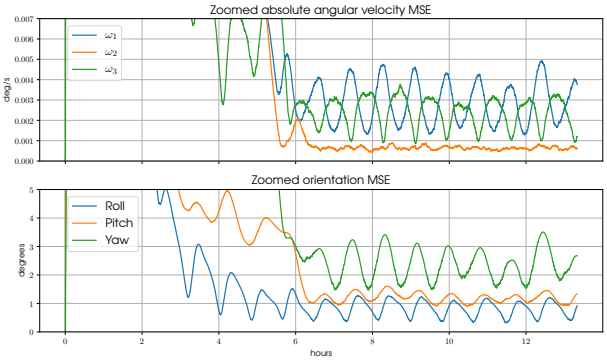

Fig. 7: Orientation and angular velocities MSEs for a satellite a in swarm, using the interpolated estimates instead of direct measurements in EKF

It can be seen that the MSEs of the Euler angles

decreased by 15% in comparison with single-satellite result, which is really good outcome for the interpolated estimates usage in a slightly perturbed environment.

5. Conclusion

In this paper we showed that even for a four-satellite formation, distributed measurements and appropriate interpolation methods can produce accurate instantaneous maps of the measured quantity. We constructed the non-degenerating tetrahedral CubeSat formation with relative motion. We outlined the procedure of how the Kriging interpolation can be carried out, studied different semivariogram models and separated them into the atlas, depending on the current sector of the orbit. We acquired empirical semivariograms for the IGRF-13 model of the geomagnetic field and fitted into them best possible model function, which was proven empirically. We found that usage of interpolated estimates in the formation of CubeSats can enhance the accuracy of the attitude control by 15% in comparison with singleton ADCS and direct measurements. Also, the interpolations technique is more robust to out of scope environmental events, such as magnetic storms. However, the disturbances used in simulations are rather small and the in-orbit resulting MSEs are expected to be different, with greater standard deviations and non-zero means. We believe that Kriging interpolation technique is worth of the close attention from researchers of mega-constellations and distributed measurements, since this technique may have a great effect on the ADCS refining or even become universal.

6. Acknowledgement

This work is funded by RFBR, project number 19-38-90278.

References

[1] Ur Aeronomie and Patrick W. Daly. The tetrahedron quality factors of csds. 1994.

[2] A. Afanasev, A. Ivanov, A. Mahfouz, and D. Pritykin. Attitude control algorithms in a swarm of cubesats: Kriging interpolation and coordinated data exchange. *Submitted to: Advances in the Astronautical Sciences*, 2020 in press.

[3] Carles Araguz, Elisenda Bou-Balust, and Eduard Alarcón. Applying autonomy to distributed satellite systems: Trends, challenges, and future prospects. *Systems Engineering*, 21(5):401–416, 2018.

[4] A.A. Chernyshov, D.V. Chugunin, M.M. Mogilevsky, and et al. Approaches to studying the multiscale ionospheric structure using nanosatellites. *Geomagnetism and Aeronomy*, 56(1):72–79, 2016.

[5] Erwan Thébault et al. International geomagnetic reference field: the 12th generation. *Earth, Planets and Space*, 67:79, 2015.

[6] A. Farrag, Tarek Mahmoud, and Ahmed Y. EL-Raffiei. Satellite swarm survey and new conceptual design for earth observation applications. *The Egyptian Journal of Remote Sensing and Space Science*, 2019.

[7] Fabrizio Fiore, Luciano Burderi, Tiziana Di Salvo, Marco Feroci, Claudio Labanti, Michelle R. Lavagna, and Simone Pirrotta. HERMES: a swarm of nano-satellites for high energy astrophysics and fundamental physics. In Jan-Willem A. den Herder, Shouleh Nikzad, and Kazuhiro Nakazawa, editors, *Space Telescopes and Instrumentation 2018: Ultraviolet to Gamma Ray*, volume 10699. International Society for Optics and Photonics, SPIE, 2018.

[8] George William Hill. Researches in the lunar theory. *American journal of Mathematics*, 1(1):5–26, 1878.

[9] DS Ivanov, M Yu Ovchinnikov, VI Penkov, DS Roldugin, DM Doronin, and AV Ovchinnikov. Advanced numerical study of the three-axis magnetic attitude control and determination with uncertainties. *Acta Astronautica*, 132:103–110, 2017.

[10] Götz Paschmann and Patrick W. Daly. Analysis Methods for Multi-Spacecraft Data. ISSI Scientific Reports Series SR-001, ESA/ISSI, Vol. 1. ISBN 1608-280X, 1998. *ISSI Scientific Reports Series*, 1, January 1998.

[11] R.E. Kalman, R.S. Bucy. New results in linear filtering and prediction theory. *Trans. ASME, Ser. D. J. Basic Eng.*, 83:95–108, 1961.

[12] T.C. Bailey, A.C. Gatrell. *Interactive Spatial Data Analysis*. Routledge, Informa PLC, 5 Howick Place, London, 1st edition, 1995.

[13] H. Wackernagel. *Multivariate Geostatistics*. Springer, Berlin, Heidelberg., 1995.

[14] RS Wiltshire and WH Clohessy. Terminal guidance system for satellite rendezvous. *Journal of the Aerospace Sciences*, 27(9):653–658, 1960.